arXiv:1202.2030v1 [nucl-th] 9 Feb 2012

New insights into antikaon-nucleon scattering and the structure of the $\Lambda(1405)$

Maxim Mai[a], Ulf-G. Meißner[a,b]

[a]Universität Bonn, Helmholtz-Institut für Strahlen- und Kernphysik (Theorie) and Bethe Center for Theoretical Physics, D-53115 Bonn, Germany
[b]Forschungszentrum Jülich, Institut für Kernphysik, Institute for Advanced Simulation, and Jülich Center for Hadron Physics, D-52425 Jülich, Germany

---

Abstract

We perform a combined analysis of antikaon-nucleon scattering cross sections and the recent SIDDHARTA kaonic hydrogen data in the framework of a coupled-channel Bethe-Salpeter approach at next-to-leading order in the chiral expansion of the effective potential. We find a precise description of the antikaon-proton scattering amplitudes and are able to extract accurate values of the scattering lengths, $a_0 = -1.81^{+0.30}_{-0.28} + i\,0.92^{+0.29}_{-0.23}$ fm , $a_1 = +0.48^{+0.12}_{-0.11} + i\,0.87^{+0.26}_{-0.20}$ fm. We also discuss the two-pole structure of the $\Lambda(1405)$.

Keywords: Kaon–baryon interactions, Baryon resonances
PACS: 13.75.Gx, 12.39.Fe, 13.75.Jz, 14.20.Jn

---

1. Introduction and summary

With the recent precise measurement of the characteristics of kaonic hydrogen by the SIDDHARTA collaboration [1], an accurate determination of the so important antikaon-nucleon scattering amplitude is now possible. The appropriate framework to perform this task is unitarized chiral perturbation theory, which combines the strictures from the chiral SU(3) dynamics of QCD with coupled channel effects, that e.g. generate the much discussed $\Lambda(1405)$ resonance, as first pointed out by Dalitz and Tuan [2]. From earlier studies by various groups, it is already known that simply taking the leading order chiral interactions in the effective potential of the respective scattering equation is insufficient to achieve the desired accurate theoretical description, see e.g. Refs. [3, 4, 5]. In fact, Ikeda et al. [6, 7] have performed such a combined analysis based on the next-to-leading order chiral effective meson-baryon Lagrangian, nicely demonstrating that indeed a more precise description of the K^-p and K^-n interaction arises. Here, we perform a similar analysis, but in contrast to Refs. [6, 7], we use a Bethe-Salpeter framework without an on-shell approximation for the intermediate meson-baryon states (as described in more detail below). The framework we use has already been successfully applied to pion-nucleon scattering in the s-waves [8] and thus it is evident to extend this analysis to antikaon-nucleon scattering. We also point out that the constraints from SIDDHARTA on the kaon-deuteron scattering length have been investigated in [9].

The main results of our investigation can be summarized as follows:

- Fitting the scattering data for $K^-p \to K^-p$, $\bar{K}^0 n$, $\Sigma^\pm\pi^\mp$, and $\Sigma^0\pi^0$ for laboratory momenta $p_{\rm lab} \leq 300$ MeV together with the SIDDHARTA data allows for a good description of the antikaon-proton cross section data (cf. Fig. 1) and an accurate determination of the scattering lengths, cf. Eq. (6).
- We can give a precise prediction for the real and imaginary part of the $K^-p \to K^-p$ scattering amplitude for center-of-mass energies $1330\,{\rm MeV} \leq W_{\rm cms} \leq 1450\,{\rm MeV}$, cf. Fig. 4.
- We have investigated the two-pole structure of the $\Lambda(1405)$ [10, 11]. While the first pole is in agreement with other determinations, we find the real part of the second pole at larger energies than usually obtained. We trace this back to the fitting procedures in other works that restrict the NLO contributions to come out close to the solution given by the Weinberg-Tomozawa term, while we do not impose such a restriction.

2. Framework

The starting point of our work is the recent analysis of πN scattering, presented in [8]. In this section we describe the basic ingredients of this approach.

In chiral perturbation theory the meson-baryon interaction at the leading chiral order is encoded in the following Lagrangian

$$\mathcal{L}^{(1)}_{\phi B} = \langle \bar{B}(i\gamma_\mu D^\mu - m_0)B\rangle + \frac{D/F}{2}\langle \bar{B}\gamma_\mu\gamma_5[u^\mu, B]_{+/-}\rangle\,, \qquad (1)$$

where $\langle \ldots \rangle$ denotes the trace in flavor space, $D_\mu B := \partial_\mu B + \frac{1}{2}[[u^\dagger, \partial_\mu u], B]$, m_0 is the baryon octet mass in the chiral SU(3) limit, and D, F are the axial coupling constants. The relevant degrees of freedom are the Goldstone bosons described by the traceless meson matrix ϕ, which is included in the above Lagrangian via $u^2 := \exp(i\phi/F_0)$ and $u^\mu := iu^\dagger\partial^\mu u - iu\partial^\mu u^\dagger$. Here, F_0 is the meson decay constant in the chiral limit. The low-lying baryons are collected in the traceless matrix B. We set the external currents to zero except for the scalar one, which is set equal to the quark mass matrix, i.e. $s = \mathcal{M} := \mathrm{diag}(m_u, m_d, m_s)$. We furthermore use $\chi_\pm := u^\dagger\chi u^\dagger \pm u\chi^\dagger u$ and $\chi := 2B_0 s$, where

Preprint submitted to Elsevier *February 10, 2012*

the constant B_0 is related to the quark condensate in the chiral limit.

Starting from the covariant derivative $D_\mu B$, the so-called Weinberg-Tomozawa term can be derived. This term dominates the s-wave interaction near the thresholds, therefore in most chiral unitary approaches the meson-baryon interaction is restricted to this term. Secondly, a meson can couple to a baryon via the axial vector current $\sim D, F$, generating the s- and u-channel exchanges of the intermediate baryons. The inclusion of these so-called Born graphs in the driving term of the Bethe-Salpeter equation leads to conceptional and practical difficulties, which are described in detail in Ref. [8, 12]. The latter are usually overcome, making use of the on-shell approximation or via projection of the kernel to the s-wave, see e.g. Ref. [5] and Ref. [6] for a more recent study. However the particular attention of the present work lies on the solution of the Bethe-Salper equation with the full off-shell dependence. Thus we will restrict the interaction kernel to a sum of contact terms, but refrain from the approximations mentioned above.

Aside from the Weinberg-Tomozawa term, we will take into account the full set of meson-baryon vertices from the second-order chiral Lagrangian. The pertinent Lagrangian density was first constructed in [13] and reads in its minimal form [14]

$$\begin{aligned}\mathcal{L}^{(2)}_{\phi B} &= b_{D/F}\langle \overline{B}[\chi_+, B]_\pm\rangle + b_0\langle \overline{B}B\rangle\langle\chi_+\rangle \\ &+ b_{1/2}\langle \overline{B}\big[u_\mu, [u^\mu, B]_\mp\big]\rangle + b_3\langle \overline{B}\big\{u_\mu, \{u^\mu, B\}\big\}\rangle + b_4\langle \overline{B}B\rangle\langle u_\mu u^\mu\rangle \\ &+ ib_{5/6}\langle \overline{B}\sigma^{\mu\nu}\Big[[u_\mu, u_\nu], B\Big]_\mp\rangle + ib_7\langle \overline{B}\sigma^{\mu\nu}u_\mu\rangle\langle u_\nu B\rangle \\ &+ \frac{i\,b_{8/9}}{2m_0}\Big(\langle \overline{B}\gamma^\mu\big[u_\mu, [u_\nu, [D^\nu, B]]_\mp\big]\rangle + \langle \overline{B}\gamma^\mu\big[D_\nu, [u^\nu, [u_\mu, B]]_\mp\big]\rangle\Big) \\ &+ \frac{i\,b_{10}}{2m_0}\Big(\langle \overline{B}\gamma^\mu\big\{u_\mu, \{u_\nu, [D^\nu, B]\}\big\}\rangle + \langle \overline{B}\gamma^\mu\big[D_\nu, \{u^\nu, \{u_\mu, B\}\}\big]\rangle\Big) \\ &+ \frac{i\,b_{11}}{2m_0}\Big(2\langle \overline{B}\gamma^\mu[D_\nu, B]\rangle\langle u_\mu u^\nu\rangle \\ &\qquad\qquad + \langle \overline{B}\gamma^\mu B\rangle\langle [D_\nu, u_\mu]u^\nu + u_\mu[D_\nu, u^\nu]\rangle\Big)\,, \qquad (2)\end{aligned}$$

with the b_i the pertinent dimension-two low energy constants (LECs). The LECs $b_{0,D,F}$ are the so-called *symmetry breakers*, while the b_i ($i = 1, \ldots, 11$) are referred to as *dynamical* LECs. On the one hand such terms may lead to sizable corrections to the leading-order result, see e.g. [15] for the calculation of meson-baryon scattering lengths up to the third chiral order. On the other hand, including such terms with full off-shell dependence we hope to account for some of the structures created by the missing Born graphs. Let us denote the in- and out-going meson momenta by q_1 and q_2, respectively. The overall four-momentum is given by $p = q_1 + p_1 = q_2 + p_2$, where p_1 and p_2 are the momenta of in- and out-going baryon, respectively. Separating the momentum space from the channel space structures, the chiral potential considered here takes the form:

$$\begin{aligned}V(\not{q}_2, \not{q}_1; p) = {}& A_{WT}(\not{q}_1 + \not{q}_2) \\ & + A_{14}(q_1 \cdot q_2) + A_{57}[\not{q}_1, \not{q}_2] + A_M \\ & + A_{811}\big(\not{q}_2(q_1 \cdot p) + \not{q}_1(q_2 \cdot p)\big),\end{aligned}$$

where the first matrix A_{WT} only depends on the meson decay constants $F_{\pi,K}$, whereas A_{14}, A_{57}, A_{811} and A_M also contain the NLO LECs as specified in appendix A. In going from the Lagrangian Eq. (2) to the above vertex rule, we have left out some terms, which are formally of third chiral order. The channel space is defined in accordance with the quantum numbers as well as the energy range of interest. For the purpose of gaining some insight on the nature of $\Lambda(1405)$ it is spanned by six vectors corresponding to the following meson-baryon states: $\{K^-p;\ \overline{K}^0 n;\ \pi^0\Lambda;\ \pi^0\Sigma^0;\ \pi^+\Sigma^-;\ \pi^-\Sigma^+\}$. The influence of other much heavier channels will be absorbed in the LECs to be fitted.

The strict perturbative chiral expansion is only applicable at low energies and certainly fails in the vicinity of (subthreshold) resonances. We extend the range of applicability by means of a coupled channel Bethe-Salpeter equation (BSE). Introduced in Ref. [16] it has been proven to be very useful both in the purely mesonic and also in the meson-baryon sector. In contrast to perturbative calculations this approach implements two-body unitarity exactly and in principle allows to generate resonances dynamically. For the meson-baryon scattering amplitude $T(\not{q}_2, \not{q}_1; p)$ and the chiral potential $V(\not{q}_2, \not{q}_1; p)$ the integral equation to be solved reads

$$\begin{aligned}T(\not{q}_2, \not{q}_1; p) ={}& V(\not{q}_2, \not{q}_1; p) + \\ & i\int \frac{d^d l}{(2\pi)^d} V(\not{q}_2, \not{l}; p) S(\not{p} - \not{l})\Delta(l) T(\not{l}, \not{q}_1; p),\end{aligned} \qquad (3)$$

where S and Δ represent the baryon (of mass m) and the meson (of mass M) propagator, respectively, and are given by $iS(\not{p}) = i/(\not{p} - m + i\epsilon)$ and $i\Delta(k) = i/(k^2 - M^2 + i\epsilon)$. Moreover, T, V, S and Δ in the last expression are matrices in the channel space.

To treat the loop diagrams appearing in the BSE Eq. (3), we utilize dimensional regularization. The purely baryonic integrals are set to zero from the beginning. In the spirit of our previous work [8], we apply the usual $\overline{\text{MS}}$ subtraction scheme, keeping in mind that the modified loop integrals are still scale-dependent. The scale μ reflects the influence of the higher-order terms not included in our potential. It is used as a fitting parameter of our approach.

The solution of the BSE Eq. (3) with full off-shell dependence is obtained following the construction principles described in Ref. [8]. As an extension of this approach we wish also to address an other issue here, namely analyticity. Let us first start with the one-meson-one-baryon loop-function $I_{MB}(s = p^2)$ in four dimensions.

$$I_{MB}(s) := \int \frac{d^4 l}{(2\pi)^4}\frac{1}{l^2 - M^2}\frac{1}{(p - l)^2 - m^2}$$

Applying the Cutkosky rules, one immediately obtains the imaginary part of this integral, given by $-(q_{\rm cms}(p^2))/(8\pi\sqrt{s})$ for $q^2_{\rm cms} = \big((s - (m + M)^2)(s - (m - M)^2)\big)/(4s)$. Keeping in mind the high energy behavior of the function $I_{MB}(s)$, we can obtain the real part of it via a subtracted dispersion relation

$$\text{Re}(I_{MB}(s)) = \text{Re}(I_{MB}(s_0)) + \frac{(s - s_0)}{\pi}\int_{s_{\rm thr}}^{\infty} ds' \frac{\text{Im}\,(I_{MB}(s'))}{(s - s')(s - s_0)},$$

where $s_{\rm thr} = (M+m)^2$ and s_0 is a subtraction point chosen to not lie on the integration contour. The solution of the BSE Eq. (3) corresponds to a bubble sum, containing exactly the same one loop-functions I_{MB}. Thus one should in principle be able to write an equation similar to the last one for the scattering amplitude

$$\mathrm{Re}(T(s)) = \mathrm{Re}(T(s_0)) + \frac{(s-s_0)}{\pi}\int_{s_{\rm thr}}^{\infty} ds' \frac{\mathrm{Im}\,(T(s'))}{(s-s')(s-s_0)}, \quad (4)$$

where for the moment we have suppressed the $\not{q}_{1,2}$ dependence. To the best of our knowledge, it is not possible to implement the last relation Eq. (4) into the BSE Eq. (3) directly. To put it in other words, the BSE ansatz is known to produce poles on the physical Riemann sheet, which are forbidden by the postulate of maximal analyticity. Thus a scattering amplitude, which solves the Eq. (3), does not satisfy Eq. (4).

Nevertheless it is possible to find a solution of the BSE Eq. (3), which fulfills Eq. (4) at least approximately, as we wish to describe now. One way to do so is to keep only those solutions of the BSE, which do not produce poles on the first Riemann sheet 'near' the real (physical) axis. E.g. in Ref. [5] solutions producing poles for $\mathrm{Im}(W_{\rm cms} = \sqrt{s}) < 250$ MeV were excluded by hand. To overcome such unsatisfactory intervention into the fitting procedure we proceed differently. First, for a fixed s and s_0 we define the following quantity

$$\chi^2_{\rm DISP} = \left(\frac{\mathrm{Re}\,(T(s) - T(s_0)) - \frac{(s-s_0)}{\pi}\int_{s_{\rm thr}}^{\infty} ds' \frac{\mathrm{Im}\left(T(s')\right)}{(s-s')(s-s_0)}}{\mathrm{Re}\,(T(s) - T(s_0))} \right)^2 . \quad (5)$$

Then the fitting parameters of our model are adjusted to minimize the quantity $\chi^2_{\rm FULL} = \chi^2_{\rm DISP} + \chi^2_{\rm DATA}$, where the latter is based on the experimental data. It should be clear that such a procedure is not suited to overcome the unphysical poles. It ensures, however, that they are moved far away from the real axis in a systematic manner, without manual intervention. This we consider an improvement of the model.

3. Fit strategy

We are now able to confront our approach with the experimental results. Throughout the present work we use the following numerical values (in GeV) for the masses and the meson decay constants: $F_\pi = 0.0924$, $F_K = 0.113$, $M_{\pi^0} = 0.135$, $M_{\pi^{+/-}} = 0.1396$, $M_{K^-} = 0.4937$, $M_{\bar{K}^0} = 0.4977$, $m_p = 0.9383$, $m_n = 0.9396$, $m_\Lambda = 1.1157$, $m_{\Sigma^0} = 1.1926$, $m_{\Sigma^+} = 1.1894$ and $m_{\Sigma^-} = 1.1975$. The baryon mass in the chiral limit, m_0 in Eq. (2), can be fixed to 1 GeV without loss of generality, as any other value only amounts to a rescaling of the unknown LECs.

Secondly, for the experimental data we consider total cross sections for the processes $K^-p \to \{K^-p, \bar{K}^0n, \pi^0\Sigma^0, \pi^+\Sigma^-, \pi^-\Sigma^+\}$ taken from Refs. [17, 18, 19, 20]. Moreover, we consider the following decay ratios

$$\gamma = \frac{\Gamma(K^-p \to \pi^+\Sigma^-)}{\Gamma(K^-p \to \pi^-\Sigma^+)} = 2.38 \pm 0.04,$$
$$R_n = \frac{\Gamma(K^-p \to \pi^0\Lambda)}{\Gamma(K^-p \to \text{neutral states})} = 0.189 \pm 0.015,$$
$$R_c = \frac{\Gamma(K^-p \to \pi^+\Sigma^-, \pi^-\Sigma^+)}{\Gamma(K^-p \to \text{inelastic channels})} = 0.664 \pm 0.011,$$

where the first one is taken from Ref. [21] and the last two from Ref. [22]. Additionally to these quite old date we use a recent determination of the energy shift and width of the kaonic hydrogen in the 1s state, i.e. $\Delta E - i\Gamma/2 = (283 \pm 42) - i(271 \pm 55)$ eV from the SIDDHARTA experiment at DAΦNE [1]. These are related to the K^-p scattering length via the modified Deser-type relation [23]

$$\Delta E - i\Gamma/2 = -2\alpha^3\mu_c^2 a_{K^-p}\left[1 - 2a_{K^-p}\alpha\mu_c(\ln\alpha - 1)\right],$$

where $\alpha \simeq 1/137$ is the fine-structure constant, μ_c is the reduced mass and a_{K^-p} the scattering length of the K^-p system.

There are 17 free parameters in the present approach. First of all, the low-energy constants represent the heavy degrees of freedom of QCD, which are integrated out. Thus they have to be fixed in a fit to the experimental data. As a matter of fact, the fitting parameters of our approach correspond to the SU(3) low-energy constants, renormalized by the effects of the not included channels $\{\eta\Lambda; \eta\Sigma^0; K^+\Xi^-; K^0\Xi^0\}$. Additionally, three subtraction constants have to be determined from a fit, which correspond to the logarithms of the undetermined regularization scales $\{\mu_{\pi\Lambda}, \mu_{KN}, \mu_{\pi\Sigma}\}$.

To reproduce the experimental data as well as to preserve the property of analyticity as described in above, we minimize the following quantity $\chi^2_{\rm FULL} = \chi^2_{\rm DISP} + \chi^2_{\rm DATA}$, where the first part is given in the Eq. (5) and the second part by the quantity

$$\chi^2_{\rm DATA} := \frac{\chi^2}{\rm d.o.f} = \frac{\sum_i n_i}{N(\sum_i n_i - p)} \sum_i \frac{\chi_i^2}{n_i}.$$

Here p is the numbers of the free parameters, n_i is the number of data points available for the observable i and N is the number of observables. The present choice of $\chi^2_{\rm DATA}$ is crucial to ensure the equal weight of different observables, independently of the corresponding number of data points. The minimization itself is performed using MINUIT [24], especially the migrad strategy in two steps, which is due to the quite complicated structure of the BSE solution with full off-shell dependence. First, parameters are found to minimize the $\chi^2_{\rm FULL}$ in the on-shell parametrization. In the second step we turn on the "off-shellness" slowly, minimizing in each step the $\chi^2_{\rm DATA}$ and taking the parameters of the best fit from the previous step as starting values. Such a procedure guarantees preservation of the right analytic properties of the solution, found in the first step.

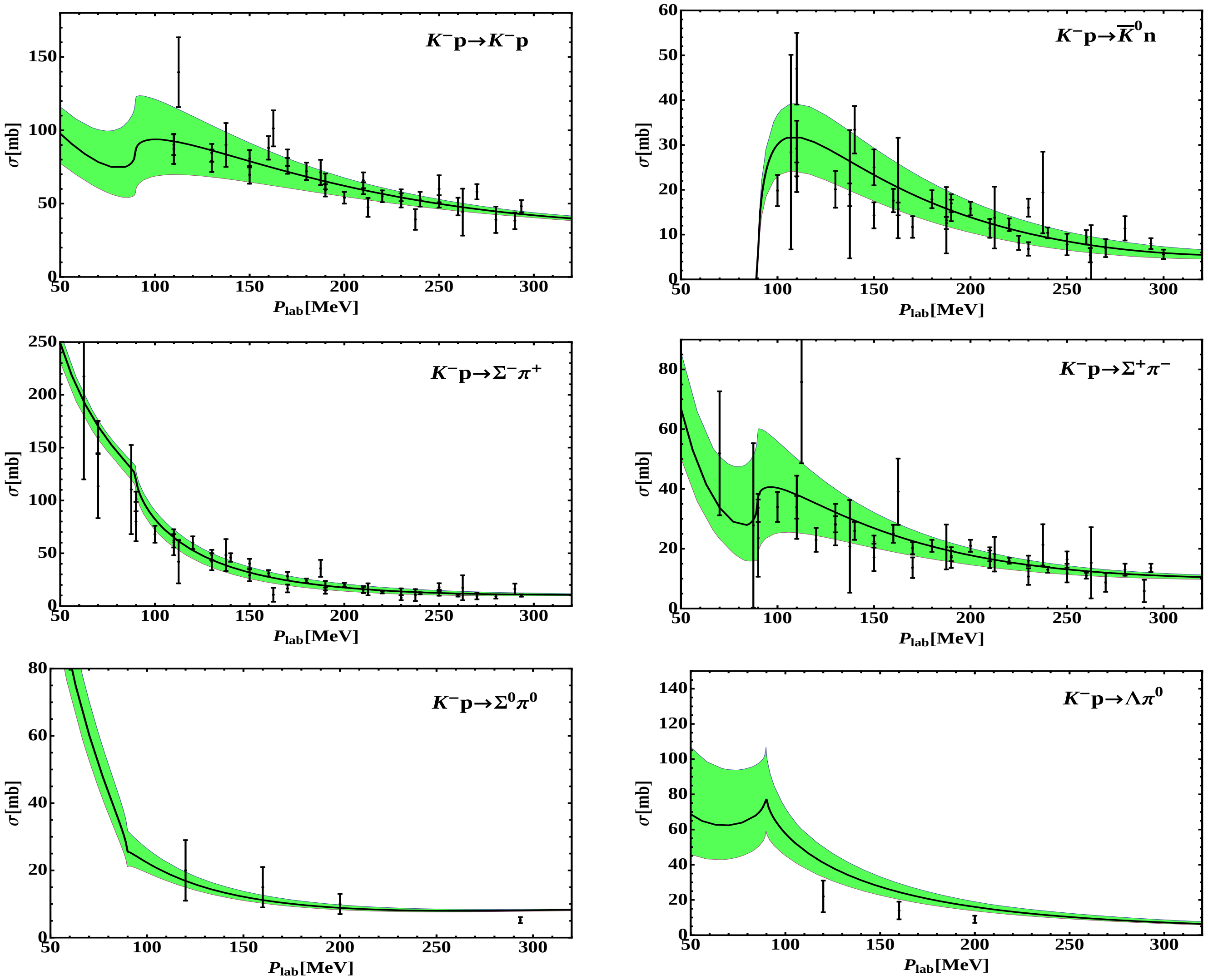

Figure 1: Total cross sections for the scattering of K^-p to various channels versus the K^- laboratory momentum. The black points with error bars denote the experimental data from [17, 18, 19, 20] considered for the fits. Shaded (green) bands denote the 1σ error bands calculated as described in the text. The reaction $K^-p \to \Lambda\pi^0$ is not a part of our fit and presented here only for completeness.

4. Results

For the best fit $\tilde{\chi}^2_{DATA} = 0.524$ we obtain the following parameter set (all b_i in GeV^{-1} and μ_i in GeV)

$\log(\mu_{KN}/(1\text{GeV}))$	$= +1.155 \pm 0.181$
$\log(\mu_{\pi\Sigma}/(1\text{GeV}))$	$= -0.008 \pm 0.002$
$\log(\mu_{\pi\Lambda}/(1\text{GeV}))$	$= -0.010 \pm 0.003$
$b_1 = +0.582 \pm 0.052$	$b_8 = -0.332 \pm 0.045$
$b_2 = -0.310 \pm 0.092$	$b_9 = +0.298 \pm 0.087$
$b_3 = +0.227 \pm 0.038$	$b_{10} = +0.198 \pm 0.058$
$b_4 = -0.939 \pm 0.069$	$b_{11} = +0.516 \pm 0.058$
$b_5 = +0.023 \pm 0.007$	$b_0 = +0.710 \pm 0.211$
$b_6 = +0.001 \pm 0.001$	$b_D = -0.291 \pm 0.068$
$b_7 = -2.518 \pm 0.110$	$b_F = -0.057 \pm 0.014$

We note that the LECs are all of natural size, indicating that all relevant physical mechanisms are included in the calculations. The experimental data on total cross sections is reproduced quite nicely, see Fig.1. We first wish to remark that due to insufficient number of data points the channel $K^-p \to \Lambda\pi^0$ is not considered as experimental input in the fit procedure. For completeness, we present the outcome of our approach for this channel in Fig.1. Secondly, all of the cross sections presented here are due to the strong interaction only. Additionally, Coulomb interaction was taken into account in [5, 7] via a non-relativistic quantum mechanical formula. Since this alone can-not count for an interference between the strong and the electromagnetic interactions, we relegate the proper inclusion of the electromagnetic contributions to a future publication.

The confidence bands presented in the above figure and the errors on further observables are calculated as follows: first we generate a large number (~ 10,000) of randomly distributed parameter sets in the error region given above. Then for each of these parameter sets we calculate the $\chi^2_{\rm DATA}$ and keep only those

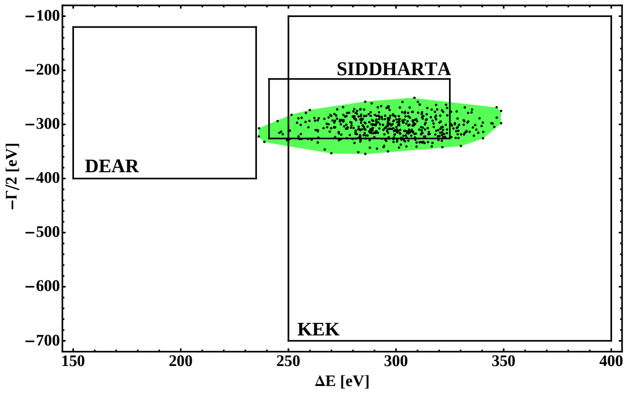

Figure 2: Energy shift and width of kaonic hydrogen as determined from the DEAR [25], the KEK [26] and the SIDDHARTA [1] experiments. The shaded area denotes the 1σ region of our approach around the best fit value.

sets, for which $\chi^2_{\rm DATA} - \tilde{\chi}^2_{\rm DATA} \leq 1.05$. Quantities calculated for these parameter sets are assumed to lie in the 1σ region around the central value.

The results for the threshold quantities are in excellent agreement with experimental data and read

$$
\begin{aligned}
\Delta E - i\Gamma/2 &= +296^{+56}_{-49} - i\,300^{+42}_{-54}\ \text{eV},\\
\gamma &= +2.44^{+0.73}_{-0.67}\,,\\
R_n &= +0.268^{+0.110}_{-0.086}\,,\\
R_c &= +0.643^{+0.015}_{-0.019}\,.
\end{aligned}
$$

As a matter of fact, the shape of the 1σ region for the energy shift and width of kaonic hydrogen cannot be assumed to be rectangular, see Fig. 2. The resulting scattering lengths for isospin $I = 0$ and $I = 1$, i.e. a_0 and a_1, are displayed in Fig. 3, in comparison to some older determinations and the determination based on scattering data alone [5]. The inclusion of the SIDDHARTA data leads to much smaller errors, especially for a_1. Our values for the scattering lengths are

$$
\begin{aligned}
a_0 &= -1.81^{+0.30}_{-0.28} + i\,0.92^{+0.29}_{-0.23}\ \text{fm}\,,\\
a_1 &= +0.48^{+0.12}_{-0.11} + i\,0.87^{+0.26}_{-0.20}\ \text{fm}\,. \qquad (6)
\end{aligned}
$$

The inclusion of the $\Lambda\pi^0$ data in the fitting procedure could yield an additional constraint on the isospin $I = 1$ amplitudes and fix the value of a_1 as done in [5]. We have not considered this channel as an experimental input for the reasons given above. The scattering length for the elastic K^-p channel reads $a_{K^-p} = -0.68^{+0.18}_{-0.17} + i\ 0.90^{+0.13}_{-0.13}$ fm. For comparison, taking the SIDDHARTA data only, one obtains $a_{K^-p} = -0.65^{+0.15}_{-0.15} + i\ 0.81^{+0.18}_{-0.18}$ fm, while Ikeda et al. find[1] $a_{K^-p} = -0.70^{+0.13}_{-0.13} + i\,0.89^{+0.16}_{-0.16}$ fm. Therefore, these fundamental chiral SU(3) parameters can now be considered to be determined with about an accuracy of ∼ 15%,

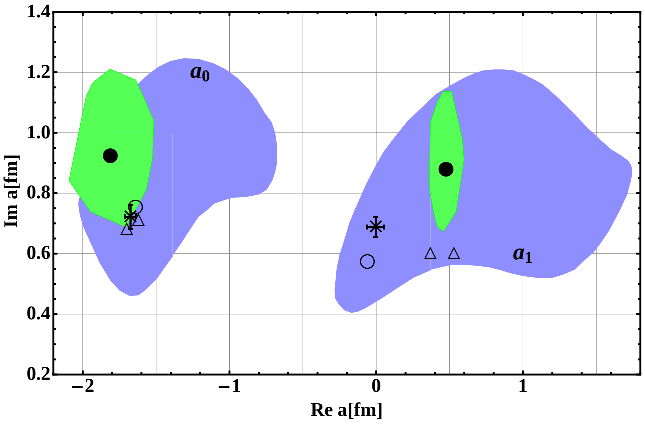

Figure 3: Real and imaginary part of isospin 0 and 1 $KN \to KN$ scattering lengths. The light shaded (green) areas correspond to the 1σ region of our approach around the central value (full circles). The darker (blue) areas correspond to the 1σ region around central value (empty circle) from Ref. [5]. the cross and empty triangles denote older experimental values from [27] and [28], respectively.

Having fixed the parameters of our model, we can extrapolate the amplitudes of elastic K^-p scattering to the subthreshold region, i.e. center-of-mass energies 1330 MeV $\leq W_{\rm cms} \leq$ 1450 MeV. The result is presented in Fig. 4. For both real and imaginary parts of the amplitude the maximum lies close to the KN threshold and is quite narrow, which indicates the presence of a close-by pole. It is also worth mentioning that the error band gets smaller to low energies, different to the recent analysis by Ikeda et al. [6, 7].

To obtain a more complete picture about the structure of $\Lambda(1405)$, the amplitudes are analytically continued to the complex $W_{\rm cms}$ plane. Microcausality forbids poles on the first Riemann sheet, that is for ${\rm Im}(W_{\rm cms}) > 0$. This is fulfilled in our model automatically due to the restoration of analyticity as described above. On the other hand some pole structure has to be responsible for the functional form of the scattering amplitudes, see Fig. 4. Two poles are found on the second Riemann sheet for isospin $I = 0$, which is achieved via analytic continuation to ${\rm Im}(W_{\rm cms}) < 0$. We denote the second Riemann sheet connected to the physical axis in the region between the $\Sigma\pi$ and $\bar{K}N$ threshold as $\mathcal{R}_{\Sigma\pi}$ and the one connected to the physical axis for $W_{\rm cms} > (M_K + m_N)$ as $\mathcal{R}_{KN}$. We find that two poles lie on different Riemann sheets, the pole position reads

$$
\begin{aligned}
\mathcal{R}_{\Sigma\pi}:\ W_1 &= 1428^{+2}_{-1} - i\,8^{+2}_{-2}\ \text{MeV}\,.\\
\mathcal{R}_{KN}:\ W_2 &= 1467^{+11}_{-7} - i\,75^{+9}_{-9}\ \text{MeV}\,.
\end{aligned}
$$

The real part of the position of the first pole agrees quite well with determination from Refs. [5, 10, 6, 7]. Its imaginary part agrees roughly with the determination of Refs. [5, 10] and is significantly smaller than extracted by Ikeda et al. [6, 7]. For the second pole, the situation is different, its imaginary part is in agreement with Refs. [5, 6, 7], but the real part is much larger.

We have investigated the origin of these observations qualitatively. First, from the analysis of πN scattering in the same

---

[1] Here, the error bars are extracted from Fig. 4 of [7].

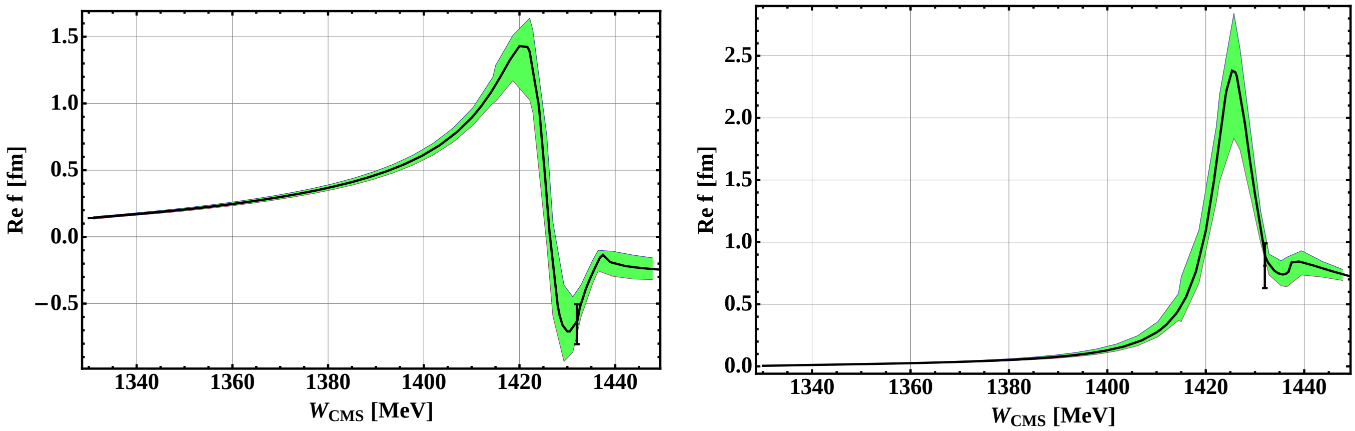

Figure 4: Real and imaginary part of the $K^- p \to K^- p$ scattering amplitude. The shaded band indicates the uncertainty of the calculation. The data point at $W_{\rm cms} = M_K + m_p$ is determined from the energy shift and width of kaonic hydrogen from the SIDDHARTA experiment.

framework, see Ref. [8], it is known that off-shell effects can account for large modifications of the pole positions. Setting the tadpole integrals to zero, we obtain immediately the solution of the BSE in the on-shell factorization. Note that this solution is still different to the one by Ikeda et al. [6, 7] since no s-wave projection is performed. We found that in the present case the off-shell effects do not alter the pole position drastically. More precisely, the imaginary part of the first pole decreases and the one of the second increases by about 10 MeV. The real parts of both poles do not change significantly. Secondly, we noticed much smaller values of the NLO LECs found by Ikeda et al. additionally to the fact that the LECs b_i ($i = 5, .., 11$) were neglected there due to the s-wave projection. To keep track of this we scale down our LECs continuously from the values found above to zero. Such a solution of the BSE is of course by no means physical since no further fitting to experimental data is done here. Qualitatively, however, we observe that both poles move (the second one by about 100 MeV) to lower values of $\mathrm{Re}(W_{\rm cms})$. The conclusion to be drawn is that difference in pole positions extracted in our approach and the one by Ikeda et al. is due to the differences in the fit strategies.

Acknowledgments

We are grateful to Peter Bruns for his stimulating remarks and cooperation. We thank Michael Döring and Wolfram Weise for comments. This work is supported in part by the DFG (SFB/TR 16 "Subnuclear Structure of Matter") and by the EU HadronPhysics3 project "Study of Strongly Interacting Matter".

Appendix A. Couplings

For the channel indices $\{b, j; i, a\}$ corresponding to the process $\phi_i B_a \to \phi_j B_b$ the relevant coupling matrices read

$$A_{WT}^{b,j;i,a} = -\frac{1}{4F_jF_i}\langle\lambda^{b\dagger}[[\lambda^{j\dagger},\lambda^i],\lambda^a]\rangle,$$

$$\begin{aligned}
A_{14}^{b,j;i,a} &= -\frac{2}{F_jF_i}\Big(2b_4\langle\lambda^{b\dagger}\lambda^a\rangle\langle\lambda^{j\dagger}\lambda^i\rangle \\
&+ b_1\Big(\langle\lambda^{b\dagger}[\lambda^{j\dagger},[\lambda^i,\lambda^a]]\rangle + \langle\lambda^{b\dagger}[\lambda^i,[\lambda^{j\dagger},\lambda^a]]\rangle\Big) \\
&+ b_2\Big(\langle\lambda^{b\dagger}\{\lambda^{j\dagger},[\lambda^i,\lambda^a]\}\rangle + \langle\lambda^{b\dagger}\{\lambda^i,[\lambda^{j\dagger},\lambda^a]\}\rangle\Big) \\
&+ b_3\Big(\langle\lambda^{b\dagger}\{\lambda^{j\dagger},\{\lambda^i,\lambda^a\}\}\rangle + \langle\lambda^{b\dagger}\{\lambda^i,\{\lambda^{j\dagger},\lambda^a\}\}\rangle\Big)\Big), \\
A_{57}^{b,j;i,a} &= -\frac{2}{F_jF_i}\Big(b_5\langle\lambda^{b\dagger}[[\lambda^{j\dagger},\lambda^i],\lambda^a]\rangle + b_6\langle\lambda^{b\dagger}\{[\lambda^{j\dagger},\lambda^i],\lambda^a\}\rangle \\
&+ b_7\Big(\langle\lambda^{b\dagger}\lambda^{j\dagger}\rangle\langle\lambda^i\lambda^a\rangle + \langle\lambda^{b\dagger}\lambda^i\rangle\langle\lambda^a\lambda^{j\dagger}\rangle\Big)\Big), \\
A_{811}^{b,j;i,a} &= -\frac{1}{F_jF_i}\Big(2b_{11}\langle\lambda^{b\dagger}\lambda^a\rangle\langle\lambda^{j\dagger}\lambda^i\rangle \\
&+ b_8\ \Big(\langle\lambda^{b\dagger}[\lambda^{j\dagger},[\lambda^i,\lambda^a]]\rangle + \langle\lambda^{b\dagger}[\lambda^i,[\lambda^{j\dagger},\lambda^a]]\rangle\Big) \\
&+ b_9\ \Big(\langle\lambda^{b\dagger}[\lambda^{j\dagger},\{\lambda^i,\lambda^a\}]\rangle + \langle\lambda^{b\dagger}[\lambda^i,\{\lambda^{j\dagger},\lambda^a\}]\rangle\Big) \\
&+ b_{10}\Big(\langle\lambda^{b\dagger}\{\lambda^{j\dagger},\{\lambda^i,\lambda^a\}\}\rangle + \langle\lambda^{b\dagger}\{\lambda^i,\{\lambda^{j\dagger},\lambda^a\}\}\rangle\Big)\Big), \\
A_{M}^{b,j;i,a} &= -\frac{1}{2F_jF_i}\Big(2b_0(\langle\lambda^{b\dagger}\lambda^a\rangle\langle[\lambda^{j\dagger}\lambda^i]\bar{\mathcal{M}}\rangle) \\
&+ b_D(\langle\lambda^{b\dagger}\{\{\lambda^{j\dagger},\{\bar{\mathcal{M}},\lambda^i\}\},\lambda^a\}\rangle + \langle\lambda^{b\dagger}\{\{\lambda^i,\{\bar{\mathcal{M}},\lambda^{j\dagger}\}\},\lambda^a\}\rangle) \\
&+ b_F(\langle\lambda^{b\dagger}[\{\lambda^{j\dagger},\{\bar{\mathcal{M}},\lambda^i\}\},\lambda^a]\rangle + \langle\lambda^{b\dagger}[\{\lambda^i,\{\bar{\mathcal{M}},\lambda^{j\dagger}\}\},\lambda^a]\rangle)\Big),
\end{aligned}$$

where λ denote the 3×3 channel matrices (e.g. $\phi = \phi^i\lambda^i$ for the physical meson fields) and the F_i are the meson decay constants in the respective channel. Moreover, $\bar{\mathcal{M}}$ is obtained from the quark mass matrix $\mathcal{M}$ via the Gell–Mann Oakes Renner relations, and given in terms of the meson masses as follows, $\bar{\mathcal{M}} = \frac{1}{2}\mathrm{diag}(M^2_{K^+} - M^2_{K^0} + M^2_{\pi^0}, M^2_{K^0} - M^2_{K^+} + M^2_{\pi^0}, M^2_{K^+} + M^2_{K^0} - M^2_{\pi^0})$.

References

[1] M. Bazzi, *et al.*, Phys. Lett. B **704** (2011) 113, [arXiv:1105.3090 [nucl-ex]].

[2] R. H. Dalitz and S. F. Tuan, Annals Phys. **10** (1960) 307.

[3] B. Borasoy, R. Nissler and W. Weise, Eur. Phys. J. A **25** (2005) 79, [hep-ph/0505239].

[4] J. A. Oller, Eur. Phys. J. A **28** (2006) 63, [hep-ph/0603134].

[5] B. Borasoy, U.-G. Meißner and R. Nissler, Phys. Rev. C **74** (2006) 055201, [hep-ph/0606108].
[6] Y. Ikeda, T. Hyodo and W. Weise, Phys. Lett. B **706** (2011) 63, [arXiv:1109.3005 [nucl-th]].
[7] Y. Ikeda, T. Hyodo and W. Weise, arXiv:1201.6549 [nucl-th].
[8] P. C. Bruns, M. Mai, U.-G. Meißner, Phys. Lett. **B697** (2011) 254, arXiv:nucl-th/1012.2233.
[9] M. Döring and U.-G. Meißner, Phys. Lett. B **704** (2011) 663, [arXiv:1108.5912 [nucl-th]].
[10] J. A. Oller and U.-G. Meißner, Phys. Lett. B **500** (2001) 263, [hep-ph/0011146].
[11] D. Jido, J. A. Oller, E. Oset, A. Ramos and U.-G. Meißner, Nucl. Phys. A **725** (2003) 181, [nucl-th/0303062].
[12] M. Mai, P. C. Bruns, U.-G. Meißner, *work in progress*.
[13] A. Krause, Helv. Phys. Acta **63** (1990) 3.
[14] M. Frink and U.-G. Meißner, JHEP **0407** (2004) 028, [arXiv:hep-lat/0404018].
[15] M. Mai, P. C. Bruns, B. Kubis and U.-G. Meißner, Phys. Rev. D **80** (2009) 094006, [arXiv:0905.2810 [hep-ph]].
[16] E. E. Salpeter and H. A. Bethe, Phys. Rev. **84** (1951) 1232.
[17] J. Ciborowski, *et al.*, J. Phys. G **8** (1982) 13.
[18] W. E. Humphrey and R. R. Ross, Phys. Rev. **127** (1962) 1305.
[19] M. Sakitt, T. B. Day, R. G. Glasser, N. Seeman, J. H. Friedman, W. E. Humphrey and R. R. Ross, Phys. Rev. **139** (1965) B719.
[20] M. B. Watson, M. Ferro-Luzzi and R. D. Tripp, Phys. Rev. **131** (1963) 2248.
[21] D. N. Tovee, *et al.*, Nucl. Phys. B **33** (1971) 493.
[22] R. J. Nowak, *et al.*, Nucl. Phys. B **139** (1978) 61.
[23] U.-G. Meißner, U. Raha and A. Rusetsky, Eur. Phys. J. C **35** (2004) 349, [hep-ph/0402261].
[24] Minuit2 released in **ROOT 5.22**/00 [http://lcgapp.cern.ch/project/cls/work-packages/mathlibs/minuit].
[25] G. Beer *et al.* [DEAR Collaboration], Phys. Rev. Lett. **94**, (2005) 212302.
[26] T. M. Ito, *et al.*, Phys. Rev. C **58** (1998) 2366.
[27] J. K. Kim, Phys. Rev. Lett. **14** (1965) 29.
[28] A. D. Martin, Nucl. Phys. B **179** (1981) 33.